Reaction-Wheel-Based Roll Stabilization for a Robotic Fish Using Neural Network Sliding Mode Control

Pengfei Zhang, Zhengxing Wu, Huijie Dong, Min Tan, and Junzhi Yu, *Senior Member, IEEE*

***Abstract*—The intrinsically reciprocating motion in fish-like propulsion causes severe attitude instability of a robotic fish, which poses enormous challenges for environmental perception and autonomous operation. To address this issue, in this article, we propose a reaction-wheel-based control framework for guaranteeing the roll stability of the robotic fish. The mechatronic design and dynamic model of the designed robotic fish with an internal rotor are presented. By means of the simplified model and frequency domain analysis, the effect factors about roll stability are concretely analyzed. More importantly, a hybrid controller that combines a sliding mode controller with a neural network feedforward compensator is developed to reject the severe disturbance on roll angle. Then, the Lyapunov stability theory is utilized to analyze the stability and convergence property of the closed-loop system. Finally, the experimental results show that the proposed methods possess more significant performances than the passive stabilization method, which provides a valuable reference for attitude stabilization control and robust environmental perception of underwater robots.**

***Index Terms*—Neural network feedforward control, reaction wheel, robotic fish, roll stability, sliding mode control.**

I. Introduction

OWING to high maneuverability, high efficiency, and noiseless performance, robotic fish holds tremendous promise for real-world applications [1], [2], such as oceanography, archaeology, and marine environmental monitoring. At present, the vast majority of existing studies of the robotic fish involve propulsive mechanisms, mechanical structures, and motion control [3]–[6]. However, the perceptual ability of the robotic fish is relatively weak, one primary reason of which is the body instability caused by the intrinsically oscillatory motion. The rhythmic oscillation of posterior body and caudal fin causes severe sway of fish body as well as introduces enormous perturbation into the measurements of onboard sensors, such as inertial sensor and camera. Taking camera as an example, the image quality may be severely damaged by motion blur due to the sway of fish body, which will bring great challenges for vision-based tasks, such as target tracking and position estimation [7]–[10].

In order to enhance the environmental perceptual ability of robotic fish, the issue of instability of fish body and onboard sensors should be tackled at first. Sun *et al.* proposed a head stability scheme to reduce the yaw sway and improve image stability by optimizing the parameters of swimming motion, but this method causes the descend of speed simultaneously [11]. To avoid the impact on swimming speed, Yang *et al.* developed a one degree-of-freedom (DoF) camera stabilizer system on yaw-axis for a robotic fish [12]. Generally, most studies focus on the solution of the instability on yaw channel, since the swing amplitude on this axis is much larger than roll and pitch. Nonetheless, even in the case of planar motion, the sway of fish body still makes severe adverse effect on roll channel, where the changing range of the roll angle can reach over 10°. At present, the common roll stabilization method in engineering is based on fixed fins, such as large pectoral fins (PF). However, the large fins may increase the drag force and its application range is narrow. Therefore, inspired by the attitude control of spacecrafts and satellites, an active reaction wheel is utilized to enhance the roll stability of the robotic fish, which not only governs the stability of fish body but also improves the validity of the onboard sensors.

The reaction wheel has been employed for the stabilization control of various robots, which provides a basic reference for our work. Gajamohan *et al.* developed a 3-D inverted pendulum based on reaction wheels, named Cubli, which can jump up from a resting position actively and balance on edge and corner [13], [14]. Lee *et al.* employed a sliding mode controller (SMC) to control a reaction wheel and implemented the balance control

Manuscript received December 29, 2019; revised February 23, 2020; accepted April 24, 2020. Date of publication May 4, 2020; date of current version August 13, 2020. This work was supported in part by the National Natural Science Foundation of China under Grant 61725305, Grant 61973303, Grant 61633020, Grant U1909206, and Grant 61421004, and in part by the Key Research Program of Frontier Sciences, CAS under Grant QYZDJ-SSW-JSC004. Recommended by Technical Editor A. Leonessa and Senior Editor X. Chen. *(Corresponding author: Junzhi Yu.)*

Pengfei Zhang, Zhengxing Wu, Huijie Dong, and Min Tan are with the State Key Laboratory of Management and Control for Complex Systems, Institute of Automation, Chinese Academy of Sciences, Beijing 100190, China, and also with School of Artificial Intelligence, University of Chinese Academy of Sciences, Beijing 100049, China (e-mail: zhangpengfei2017@ia.ac.cn; zhengxing.wu@ia.ac.cn; donghuijie2018@ia.ac.cn; min.tan@ia.ac.cn).

Junzhi Yu is with the State Key Laboratory of Management and Control for Complex Systems, Institute of Automation, Chinese Academy of Sciences, Beijing 100190, China, and also with State Key Laboratory for Turbulence and Complex Systems, Department of Mechanics and Engineering Science, BIC-ESAT, College of Engineering, Peking University, Beijing 100871, China (e-mail: junzhi.yu@ia.ac.cn).

Color versions of one or more of the figures in this article are available online at https://ieeexplore.ieee.org.

Digital Object Identifier 10.1109/TMECH.2020.2992038

on the roll channel of a unicycle robot [15]. Jin *et al.* proposed a gain-scheduling balancing-control scheme to govern the lateral balance of a one-wheel pendulum robot with a reaction wheel [16]. Zabihi *et al.* designed a one-legged handspringing robot using the balance mechanism based on the reaction wheel, which can hop with both its springy sides [17]. Whitacre *et al.* presented a spherical underwater vehicle applied for spacecraft simulation, the attitude of which is controlled by three orthogonal reaction wheels [18]. However, compared with the above robots, the stabilization control of robotic fish faces with more difficulties owing to the persistent oscillation of fish tail and complex aquatic environment, which puts forward higher requirements on the control algorithm.

This article aims to develop a feasible solution to govern the roll stability of the robotic fish. The main contributions are twofold. On the one hand, the reaction wheel is first employed for the attitude stabilization control of the robotic fish. A novel mechatronic design of the robotic fish equipped with an internal rotor and the corresponding dynamic model are proposed. Besides, the superiority of reaction-wheel-based method is theoretically analyzed compared with other methods based on mechanical optimization or large fins. On the other hand, a neural network sliding mode controller (NNSMC) is designed to address the difficulties in roll stabilization of the robotic fish, where a neural network is utilized to estimate the compensation of tail oscillation and the SMC is applied to reject the fluid disturbance and modeling error. The validity and effectiveness of the proposed methods are demonstrated in experimental results. It is revealed that the robotic fish achieves robust roll stability and the data quality of onboard sensors, such as camera, is significantly improved. The proposed methods will shed light on the attitude stabilization control of underwater robots including not only robotic fish but also autonomous underwater vehicle, glider, and etc. Further, the obtained results lay a solid foundation for underwater robots to achieve better perceptual ability and autonomous operation.

The rest of this article is organized as follows. The overall mechatronic design and modeling are provided in Section II. Section III gives the analysis of roll stability of a robotic fish. Section IV introduces the NNSMC in detail. The experimental setup and the corresponding results are offered in Section V. Finally, Section VI concludes this article.

II. Mechatronic Design and System Modeling

A. Mechatronic Design

The conceptual design and mechatronic of the robotic fish are depicted in Fig. 1. The overall robotic fish consists of three segments, including a head cabin, a reaction wheel cabin, and a caudal cabin. The head cabin, integrating a microcontroller, an inertial sensor, a power system, and a camera stabilizer, is employed to govern the motion of the robot. In particular, a micro camera is mounted at fish head for perceiving external environment and the camera stabilizer is utilized to reduce the influence of the sway of the fish head during swimming [12]. The reaction wheel cabin undertakes the function of roll stabilization, where the torque generated by the accelerative or decelerative

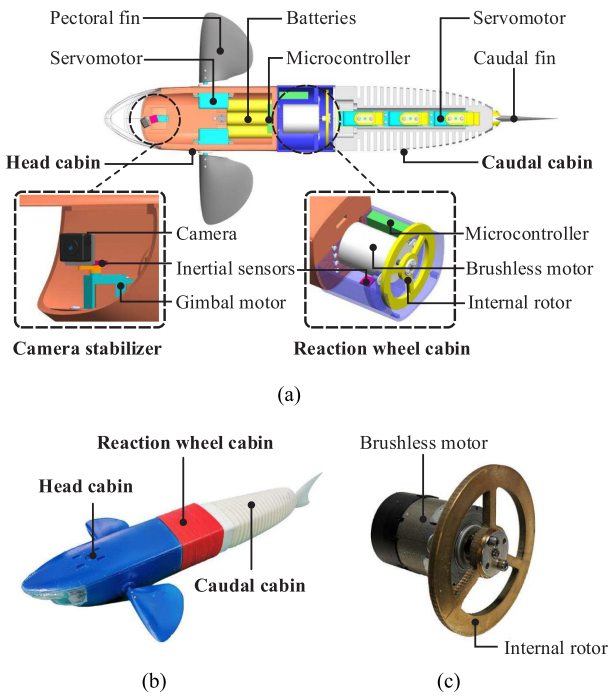

Fig. 1. Illustrations of mechatronic structure of the robotic fish. (a) Conceptual design. (b) Robotic prototype. (c) Reaction wheel.

TABLE I
Mechanical Parameters of the Developed Robotic Fish

Items	Characteristics
Size ($L \times W \times H$)	$\sim 622.79 \times 288.15 \times 87.01$ mm^3
Total mass	~ 2.335 kg
Size of rotor ($L \times W \times H$)	$\sim 80 \times 80 \times 4$ mm^3
Mass of rotor	~ 0.097 kg
Inertia of rotor	$\sim 9.9053 \times 10^{-3}$ kg $\cdot$ m^2
Material of rotor	Brass

rotation of reaction wheel is applied to avoid the disturbance. For instance, when the robotic fish is disturbed by the clockwise torque, the clockwise accelerative rotation of reaction wheel can produce counterclockwise torque to stabilize the fish body. In order to be portable to other robot platforms, the reaction wheel cabin is designed as an independent unit, which equips with individual microcontroller and inertia sensor. An internal rotor is installed in the middle of this cabin and its rotatable axis is aligned with the central axis of fish body. The rotor is directly actuated by a brushless dc motor without reduction gearbox for higher response speed and smaller volume. For the sake of obtaining larger counter-torque, the inertia of rotor is designed as large as possible in the constraints of volume and its material is chosen as the brass [19]. The caudal cabin includes a three-link tail composed by three servomotors and a caudal fin, which provides primary thrust for swimming. Besides, a pair of PF is actuated by two independent servomotors, which possesses one DoF on pitch channel. The corresponding specifications of the developed robotic fish are tabulated in Table I.

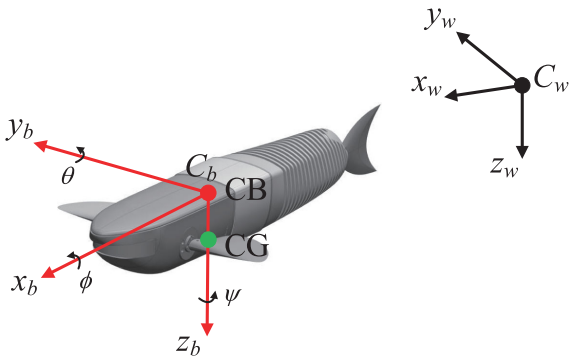

Fig. 2. Body-fixed and earth-fixed reference frames of the robotic fish.

B. Dynamic Modeling

In this section, we present a 3-D model of the robotic fish with a reaction wheel. For simplicity, the head cabin, and reaction wheel cabin are considered as a whole, where the motion equations are obtained by computing momenta from total system energy [18], [20]. The effects of three-link tail, PF, and other elements are abstracted as the external forces exerted on the body–rotor system. Besides, the fluid, in which the robotic fish is immersed, is assumed to be irrotational, incompressible, inviscid as well as that is static at the infinitely distant boundary [21]. Furthermore, we assume that the rigid head of the robotic fish is neutrally buoyant with the centers of buoyancy and gravity that are not coincident but both located at vertical line.

The earth-fixed reference frame C_w and the body-fixed reference frame C_b whose origin is located at the center of buoyancy (CB) are shown in Fig. 2. $\mathbf{r}_{bm} = [0, 0, z_{bm}]^T$ denotes the vector from the CB to the center of gravity (CG). The Euler angles, roll (ϕ), pitch (θ), and yaw (ψ), represent the attitude of C_b with respect to (w.r.t.) C_w. $\mathbf{V}_b = [v_{b,x}, v_{b,y}, v_{b,z}]^T$ and $\mathbf{\Omega}_b = [\omega_{b,x}, \omega_{b,y}, \omega_{b,z}]^T$ are defined as the translational and angular velocities of CB expressed in C_b, respectively. In addition, the spin angle of internal rotor is given by α_r and the angular velocity of rotor relative to the body-fixed frame is ω_r.

Since the change of attitude is the main consideration in this article, the kinematics of the body–rotor system can be written as follows:

$$\dot{\phi} = \omega_{b,x} + (\tan\theta \sin\phi)\omega_{b,y} + (\tan\theta \cos\phi)\omega_{b,z} \quad (1)$$

$$\dot{\theta} = (\cos\phi)\omega_{b,y} + (-\sin\phi)\omega_{b,z} \quad (2)$$

$$\dot{\psi} = (\sin\phi/\cos\theta)\omega_{b,y} + (\cos\phi/\cos\theta)\omega_{b,z} \quad (3)$$

$$\dot{\alpha_r} = \omega_r. \quad (4)$$

Treating the combined body–fluid–rotor system as a single dynamic one with kinetic energy [18], we derive the dynamic model of the whole system as below.

$$\dot{\mathscr{V}} = -\mathbf{H}^{-1}\mathbf{K}\mathscr{V} + \mathbf{H}^{-1}\mathbf{u} + \mathbf{H}^{-1}\mathscr{F} \quad (5)$$

where

$$\mathscr{V} = \begin{bmatrix} \mathbf{\Omega}_b \\ \mathbf{V}_b \\ \omega_r \end{bmatrix}, \mathbf{u} = \begin{bmatrix} \mathbf{0}_{3\times1} \\ \mathbf{0}_{3\times1} \\ T_r \end{bmatrix}, \quad \mathbf{K} = \begin{bmatrix} \hat{\mathbf{\Omega}}_b\mathbf{\Lambda}_s & \mathbf{C}_s\hat{\mathbf{\Omega}}_b & \mathbf{0}_{3\times1} \\ -\hat{\mathbf{\Omega}}_b\mathbf{C}_s & \mathbf{M}_s\hat{\mathbf{\Omega}}_b & \mathbf{0}_{3\times1} \\ \mathbf{0}_{1\times3} & \mathbf{0}_{1\times3} & 0 \end{bmatrix}$$

$$\mathbf{H} = \begin{bmatrix} \mathbf{\Lambda}_s & \mathbf{C}_s & J_r\mathbf{e}_1 \\ -\mathbf{C}_s & \mathbf{M}_s & \mathbf{0}_{3\times1} \\ J_r\mathbf{e}_1^T & \mathbf{0}_{1\times3} & J_r \end{bmatrix}, \quad \mathscr{F} = \begin{bmatrix} \sum_i \hat{\mathbf{r}}_i\mathbf{F}_{\text{ext}_i} + \mathbf{T}_{\text{ext}} \\ \mathbf{F}_{\text{ext}} \\ 0 \end{bmatrix}$$

T_r represents the internal torque of rotor and J_r denotes the rotational inertia of rotor. $\mathbf{F}_{\text{ext}}$ and $\mathbf{T}_{\text{ext}}$ represent total external forces and torques, respectively. $\mathbf{r}_i$ denotes the location vector of $\mathbf{F}_{\text{ext}_i}$, where i represents the various sources of force, including buoyancy, gravity, body hydrodynamic, caudal body, and PF [22]. Besides, $\mathbf{\Lambda}_s$ denotes the inertia of the body–fluid system with the rotor locked in place. $\mathbf{M}_s$ is the amount of the mass of entire body–rotor system. $\mathbf{C}_s = m\hat{\mathbf{r}}_{bm}$ is the coupling matrix, where $\hat{\cdot}$ denotes the skew-symmetric matrix. $\mathbf{e}_i$ denotes a 3-D unit vector where the ith element is 1.

III. Roll Stability Analysis

In order to investigate the effect factors of roll stability, the simplified model of roll channel is derived at first in this section. Further, the frequency domain analysis is utilized to demonstrate the adaptability of various stabilization methods.

A. Dynamic Model Simplification on Roll Channel

Take the planar motion into consideration, the pitch angle θ is assumed to be zero, so $\tan\theta = 0$. The change of roll angle is derived by (1), which can be described as

$$\dot{\phi} = \omega_{b,x}. \quad (6)$$

It is indicated that the rate of roll angle depends on $\omega_{b,x}$. Since the appearance of robot is nearly symmetry, the inertial matrix is assumed to be diagonal. Additionally, via matrix inversion lemma, the angular acceleration $\dot{\omega}_{b,x}$ is further derived on the basis of (5).

$$\dot{\omega}_{b,x} = B_t T_{\text{ext},x} - B_t T_r + h \quad (7)$$

where

$$B_t = \frac{M_{s,y}}{(\Lambda_{s,xx} - J_r)M_{s,y} - m^2 z_{bm}^2}$$

$$h = \frac{(\Lambda_{s,yy} - \Lambda_{s,zz})M_{s,y} - m^2 z_{bm}^2}{(\Lambda_{s,xx} - J_r)M_{s,y} - m^2 z_{bm}^2}\omega_{b,y}\omega_{b,z} + \frac{mz_{bm}}{(\Lambda_{s,xx} - J_r)M_{s,y} - m^2 z_{bm}^2}F_{\text{ext},y}$$

B_t denotes the coefficient of $T_{\text{ext},x}$ and T_r. h represents the disturbance generated by the reciprocating motion of fish tail. $\Lambda_{s,xx}$ is the first element in the diagonal of $\mathbf{\Lambda}_s$. Similarly, $M_{s,y}$ denotes the second element in the diagonal of $\mathbf{M}_s$.

Furthermore, $T_{\text{ext},x}$ provides primary passive stabilizing effect for roll channel, which includes the torques of gravity, hydrodynamic, and PF. Since pitch angle θ is assumed as zero, the x-axis component of gravity torque can be simplified as

$T_{\text{grav},x} = -mgz_{bm}\cos\theta\sin\phi = -mgz_{bm}\sin\phi$. For hydrodynamic torque and PF torque, their damping effects are proportional to angular velocity, which can be written as $T_{\text{hydro},x} = K_h\omega_{b,x}$ and $T_{\text{pect},x} = K_p\omega_{b,x}$, respectively. K_h and K_p are ratio coefficients. Then, we obtain

$$T_{\text{ext},x} = -mgz_{bm}\sin\phi + K_h\omega_{b,x} + K_p\omega_{b,x}. \tag{8}$$

Synthesizing (6)–(8), the simplified dynamic model of roll channel is derived as follows:

$$\begin{aligned}\dot{x}_1 &= x_2\\ \dot{x}_2 &= K_1\sin x_1 + K_2x_2 + K_3u + h(t)\end{aligned} \tag{9}$$

where

$$\begin{aligned}&x_1 = \phi,\ x_2 = \omega_{b,x},\ u = T_r\\ &K_1 = -mgz_{bm}B_t < 0\\ &K_2 = (K_h + K_p)B_t < 0\\ &K_3 = -B_t < 0.\end{aligned}$$

B. Stabilization Method Analysis

Since the objective of roll stabilization is to regulate the roll angle approach to zero, the characteristic of system (9) around the origin should be investigated. Specifically, the effects of K_1 and K_2 are analyzed. For this purpose, the control input is set to zero and $\sin x_1$ is linearized as x_1 near origin. Therefore, the original system can be regarded as a second-order linear system and the transfer function between $X_1(s)$ and $H(s)$ can be written as

$$G(s) = \frac{X_1(s)}{H(s)} = \frac{1}{s^2 - K_2s - K_1} \tag{10}$$

where $X_1(s)$ and $H(s)$ are Laplace transformation of $x_1(t)$ and $h(t)$, respectively.

Since the swimming motion controller is based on central pattern generator that generates sine-like motion signals, the perturbation $h(t)$ can be assumed as sinusoidal signal for the convenience of theoretical analysis [23]. Hence, the amplitude response characteristic of system can be employed to evaluate the stability of roll angle. The smaller amplitude response indicates that the roll angle is maintained within a smaller range, which means better stability. The amplitude response of system can be derived as

$$|G(j\omega)| = \frac{1}{\sqrt{\omega^4 + (K_2^2 + 2K_1)\omega^2 + K_1^2}} \tag{11}$$

where ω denotes the frequency of perturbation.

Referring to (11), the denominator should be as large as possible so that $|G(j\omega)|$ achieves minimum. Apparently, the denominator increases with the value of $|K_2|$. The larger $|K_2|$, the smaller $|G(j\omega)|$. For K_1, the denominator is a quadratic function, where ω and K_2 are regarded as constants. By analyzing this quadratic function, the minimum point is $K_1 = -\omega^2$ and the minimum value is $K_2^2\omega^2 > 0$. It is indicated that the denominator of $|G(j\omega)|$ decreases with $|K_1|$ within the range of $[0, \omega^2]$ at first, then it increases within $[\omega^2, \infty)$. Therefore, it reveals that the optimal amplitude response depends on the frequency of perturbation.

According to the analysis of K_1 and K_2, two kinds of stabilization methods are further discussed. The first method is to optimize the mechanical layout design to change K_1, such as the relative position between CG and CB. K_1 can be adjusted to be proper for some certain perturbation frequencies, but the adaptability of this method is too weak. The second method is to increase damping torque by the increment of $|K_2|$, such as employing larger PF and rough material, while it will weaken the motion performances of robot. Therefore, the reaction-wheel-based method is the better solution for the roll instability issue. Referring to (9), K_1 and K_2 can be configured arbitrarily for better amplitude response by the control input of internal rotor, which provides stronger adaptability for various scenarios. Besides, the reaction wheel is an internal actuator that possesses smaller impact on motion performances.

IV. Controller Design

In this section, a hybrid controller of SMC with the neural network feedforward compensator is designed for stabilizing the roll angle by a reaction wheel.

From the previous analysis, a simplified dynamic model with uncertainties can be obtained based on (9) as follows:

$$\begin{aligned}\dot{x}_1 &= x_2\\ \dot{x}_2 &= K_1\sin x_1 + K_2x_2 + K_3u + h(t) + d(t)\end{aligned} \tag{12}$$

where $h(t)$ represents the perturbation caused by fish swimming. The unknown uncertainties $d(t)$, consisting of modeling error and the external disturbance of fluid, are assumed to be bounded, satisfying $|d(t)| \le \gamma$ and $\gamma > 0$.

Regarding (12), by neglecting the control input u and the disturbances h and d, the remaining system is asymptotically stable for the origin. Therefore, the primary intention for controller design is to address the persistent disturbance induced by swimming and unmodeled uncertainties. For the compensation of h, the unknown motion states like velocity and modeling error make it inappropriate for calculating theoretically. Hence, a data-driven neural network feedforward controller is utilized for estimating h, where the inputs are the tail joint velocities $\dot{\theta}_{j_i}$ $(i = 1, 2, 3)$. While for the unmodeled uncertainties d, these disturbances are tackled by means of SMC, which is known as a robust method. Fig. 3 shows the block diagram of the NNSMC.

A. SMC Design

The control law of sliding mode control comprising equivalent term and switching term is shown as follows [24]–[26]:

$$u = u_{\text{eq}} + u_s. \tag{13}$$

For equivalent term, the intention is to ensure that system trajectory stays on sliding surface after reaching the sliding surface. In order to obtain equivalent control, the sliding surface of the roll control is defined as

$$s_{\text{roll}} = x_2 + Cx_1 \tag{14}$$

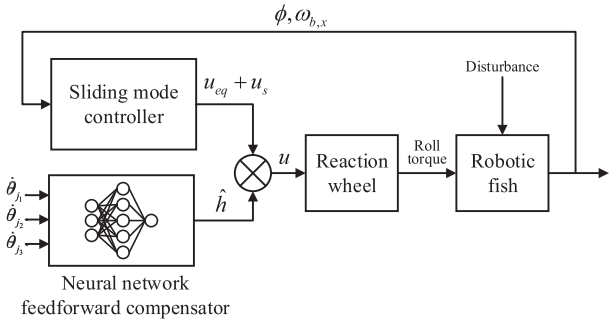

Fig. 3. Block diagram of the NNSMC.

where $C > 0$ is a positive constant that determines the slope of the sliding surface. The time derivative of s_{roll} is as follows:

$$\dot{s}_{\text{roll}} = \dot{x}_2 + C\dot{x}_1 = \dot{x}_2 + Cx_2. \tag{15}$$

By denoting $\dot{s}_{\text{roll}} = 0$, the u_{eq} is solved by (12) and (15)

$$u_{\text{eq}} = -\frac{1}{K_3}(K_1 \sin x_1 + K_2 x_2 + h + d + Cx_2). \tag{16}$$

In fact, the equivalent control usually cannot be implemented since h and d are unknown disturbances. In order to obtain the available control law, h is replaced by the estimation $\hat{h}$ of neural network and d is estimated by the high-frequency switching control $u_s = \beta \operatorname{sgn}(s_{\text{roll}})$. Additionally, for configuring system parameters as the desired values, the coefficients of $\sin x_1$ and x_2 in (16) are replaced by C_1 and C_2, respectively. Therefore, the entire control input can be calculated as

$$u = -\frac{1}{K_3}\left[C_1 \sin x_1 + C_2 x_2 + \hat{h} + \beta \operatorname{sgn}(s_{\text{roll}})\right] \tag{17}$$

where $C_1 > K_1$ and $C_2 > K_2 + C$ are controller parameters. $\hat{h}$ denotes the estimation of neural network and the estimation error $\tilde{h}$ is assumed to be bounded, satisfying $\tilde{h} = |h - \hat{h}| < \varepsilon$ and $\varepsilon > 0$. Besides, β is a positive constant and it is chosen as $\beta > \gamma + \varepsilon$.

Then, we have the following proposition.

Proposition: For $x_1 \in [-\pi/2, \pi/2]$, if the control law that designed by (17) is applied to system (12), x_1, x_2, and s_{roll} can converge to zero in finite time.

Proof: Consider the following Lyapunov function $V(x_1, s_{\text{roll}})$

$$V = -P_1(1 - \cos x_1) - \frac{1}{2}P_2 C x_1^2 + \frac{1}{2}s_{\text{roll}}^2 \tag{18}$$

where $K_1 < 0$, $K_2 < 0$, $P_1 = K_1 - C_1 < 0$, $P_2 = K_2 - C_2 + C < 0$, and $C > 0$. Obviously, $V(0,0) = 0$ and $V > 0$ for $x_1 \neq 0$ and $s_{\text{roll}} \neq 0$. The time derivative of V can be derived along with (12), (14), (15), and (17)

$$\begin{aligned}
\dot{V} &= -P_1 \dot{x}_1 \sin x_1 - P_2 C x_1 \dot{x}_1 + s_{\text{roll}} \dot{s}_{\text{roll}} \\
&= P_1 C x_1 \sin x_1 + P_2 x_2^2 + s_{\text{roll}}\left[(h - \hat{h}) + d - \beta \operatorname{sgn}(s_{\text{roll}})\right] \\
&\leq P_1 C x_1 \sin x_1 + P_2 x_2^2 + |s_{\text{roll}}|(|\tilde{h}| + |d| - \beta) \\
&\leq P_1 C x_1 \sin x_1 + P_2 x_2^2 + (\gamma + \varepsilon - \beta)|s_{\text{roll}}|.
\end{aligned} \tag{19}$$

Due to $x_1 \sin x_1 \geq 0$ for $x_1 \in [-\pi/2, \pi/2]$ and $\gamma + \varepsilon - \beta < 0$, it can be deduced that $\dot{V}$ is negative for $s_{\text{roll}} \neq 0$ and $x_1 \neq 0$ when $x_1 \in [-\pi/2, \pi/2]$. This means that $x_1 \to 0$ and $s_{\text{roll}} \to 0$ as $t \to \infty$. In addition, according to (14), $x_2 = s_{\text{roll}} - Cx_1$ converges to zero as $t \to \infty$ together with s_{roll} and x_1. Above all, the proof is completed. ■

Besides, in order to reduce the chattering phenomenon in sliding mode control, a saturation function $\operatorname{sat}(s)$ is utilized to substitute signum function. Equation (17) is updated by the following control

$$u = -\frac{1}{K_3}\left[C_1 \sin x_1 + C_2 x_2 + \hat{h} + \beta \operatorname{sat}(s_{\text{roll}})\right]. \tag{20}$$

B. Design of Neural Network Feedforward Compensator

Considering the difficulties of measuring the motion states as well as the modeling error, it is hard to derive the compensation of disturbance h directly. Therefore, the neural network algorithm is employed to estimate $\hat{h}$ as the feedforward controller [27], [28].

In order to construct neural network, a proper network input should be determined at first. In theory, the disturbance h is related to the body motion states and the tail joint states, but the body motion states are hardly obtained. Considering the body motion is generated by tail joints, the joint velocities can effectively describe the disturbance caused by fish swimming. Based on this concept, a three-layer back propagation (BP) neural network, where the inputs are joint velocities $\dot{\theta}_{j_i}$ $(i = 1, 2, 3)$ and the output is the estimation $\hat{h}$, is built as follows:

$$\hat{h} = f\left[\sum_{k=1}^{n} w_o^k f\left(\sum_{i=1}^{3} w_h^{k,i}\dot{\theta}_{j_i} + b_h^k\right) + b_o\right] \tag{21}$$

where $f(\cdot)$ is the sigmoid function. $w_h^{k,i}$ represents the weight between neuron i in input layer and neuron k in hidden layer. Similarly, w_o^k denotes the weight from hidden neuron k to output neuron. b_h^k and b_o are the bias of hidden neuron k and output neuron, respectively. n is the number of neurons in the hidden layer. Here, n is set to 5.

Furthermore, the weights and bias of the neural network are obtained through off-line training. Since the actual network output h can not be measured directly, training data is hard to be acquired. To collect reliable h, we maintain the water as calm as possible so that the fluid disturbance d approach to zero. Then, we make the control input u equal to zero and apply (22) to calculate h

$$h = \dot{x}_2 - K_1 \sin x_1 - K_2 x_2 \tag{22}$$

where x_1 and x_2 can be measured by inertial sensor as well as the linear tracking differentiator is employed to compute $\dot{x}_2$. Besides, K_1 and K_2 are obtained through system identification. The complete training processes are listed as follows:

1) Collect the system states under impulse response [Release the fish body at a certain roll angle, then record x_1 and x_2. Meanwhile, keep tail still ($h = 0$), zero control ($u = 0$), and small fluid disturbance ($d = 0$)].

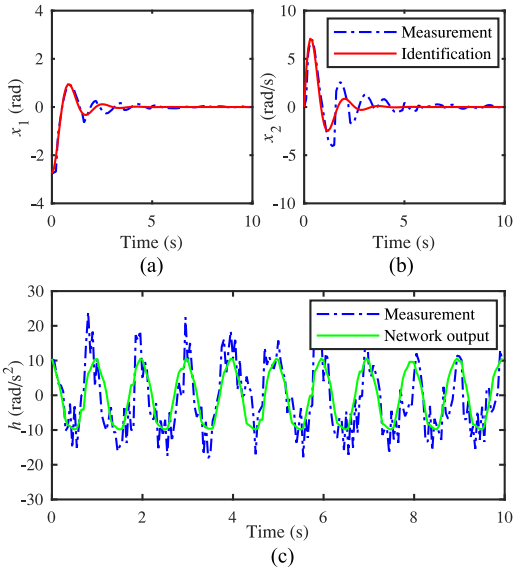

Fig. 4. Results of parameter identification and neural network training. (a) The comparison between the identified model outputs and the measurements of x_1. (b) The comparison of x_2. (c) The comparison between the neural network outputs and the actual h.

2) Identify the parameters K_1 and K_2 (The identified system equations are $\dot{x}_1 = x_2$, $\dot{x}_2 = K_1 \sin x_1 + K_2 x_2$).
3) Let robotic fish swim ($h \neq 0, u = 0, d = 0$) and collect $\dot{\theta}_{j_i}$, x_1, and x_2 synchronously.
4) Apply linear tracking differentiator to calculate $\dot{x}_2$.
5) Compute h by (22) (Suppose both u and d are zero).
6) Apply BP algorithm to train the neural network.

The results of parameter identification and offline training are depicted in Fig. 4. It is revealed that both the identified system and neural network achieve acceptable approximation accuracy.

V. Experiments

In order to assess the effectiveness of the proposed methods, we conducted a series of aquatic experiments in an indoor pool. An inertial sensor was mounted horizontally at the center of fish body to get roll angle and angular velocity of the robot. A microcontroller unit was applied to process sensor data and compute control signal at the frequency of 100 Hz.

A. Stabilization Effectiveness Comparison

It is well known that one primary function of PF for natural fish is to keep balance. Based on this intuition, large PF is widely used for the stabilization of the robotic fish by researchers. Therefore, the stabilization performances of PF and reaction wheel were compared in this section. Fig. 5(a) displays the response curve of roll angle ϕ, when the robot was released at an initial roll angle about 40° and its tail was still. The results of NNSMC show no overshoot and dramatic convergent speed compared with the system without and with large PF. In Fig. 5(b), the change of roll angle is shown during swimming with 1.0 Hz tail beat frequency (TBF). The quantitative comparison results are clearly depicted in Fig. 5(c), which shows the average range of

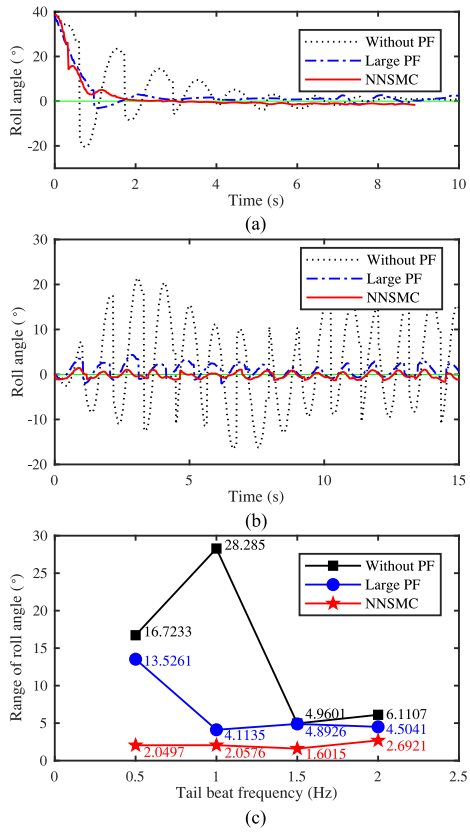

Fig. 5. Comparison about roll stability among the robotic fish without PF, with large PF and with internal rotor controlled by NNSMC. (a) Impulse response about the roll angle. (b) The change of roll angle during swimming with the TBF of 1.0 Hz. (c) The range of roll angle during swimming with various TBFs.

roll angle for three cases under various TBFs. Note that all the experiments about the average range of roll angle are conducted three times, and the worst results are presented. The range of roll angle of the system with internal rotor is depressed within 1.5°–3°, which is significantly smaller than other two cases. Especially for 0.5 Hz TBF, the range of roll angle for the case with internal rotor is only 12.26% of that without PF and 15.15% of that with large PF. Clearly, internal rotor possesses better stabilization performances in wide range of TBFs, compared with the passive stabilization method based on PF.

B. Controller Comparison

A contrast experiment was designed to verify the performances of the NNSMC method compared with that of SMC and proportional–integral–derivative (PID) controller. Note that PF was not utilized during the experiments. Fig. 6(a) depicts the change of roll angle at 1.0 Hz TBF. The fluctuation of the roll angle of NNSMC is obviously less than PID and SMC. Furthermore, the quantitative comparisons are illustrated in Fig. 6(b). Compared with the system with large PF, all controllers maintain the smaller average ranges of roll angle. But for 0.5 Hz TBF, the average ranges of PID and SMC are still too large. The NNSMC based on neural network feedforward control effectively tackles this problem, which decreases the average

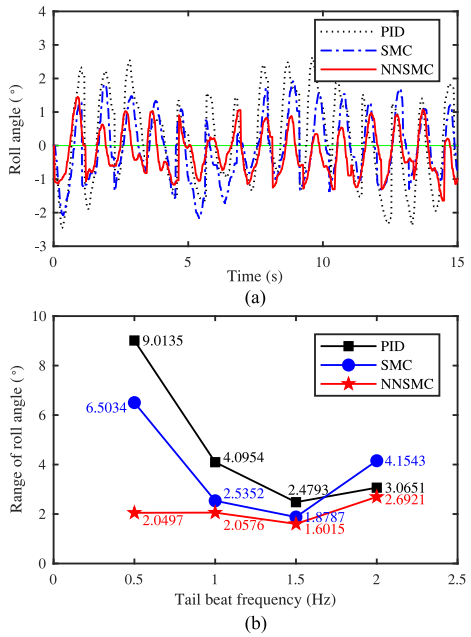

Fig. 6. Comparison about roll stability among three control methods. (a) The change of roll angle during swimming with the TBF of 1.0 Hz. (b) The range of roll angle during swimming with various TBFs.

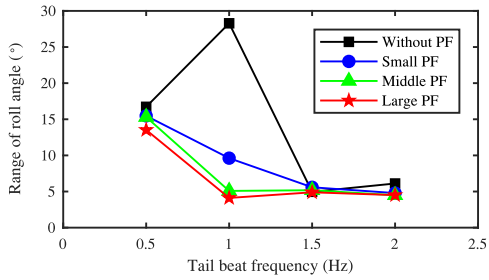

Fig. 7. Range of roll angle of the robotic fish with the different-sized PF during swimming with various TBFs.

range to 2.0497°. Besides, for other TBFs, the stabilization performances of NNSMC are also significantly superior to both PID and SMC.

C. PF Analysis

In order to further verify the necessity of reaction wheel, the limitations of PF were carefully discussed. Fig. 7 illustrates the roll stability of three different-sized and same-shaped PFs under various TBFs. A careful inspection of Fig. 7 reveals that the average ranges of all cases are very close for 0.5, 1.5, and 2.0 Hz TBFs. Although the size of PF exhibits significant effect for 1.0 Hz, it indicates that the stabilization function of PF is only efficient for a small range of TBFs.

Generally, PF also undertakes the motion function. Through deflecting the PF angle, robotic fish can achieve floating and diving. In Fig. 8, the influence of the PF angle w.r.t. the average range of roll angle is analyzed. It is obvious that the range of roll angle increases quickly with the increment of PF angle. The maximum range of roll angle achieves 12.7469° when the deflection angle is −60°. As a contrast, the reaction wheel controlled by NNSMC effectively reduces the adverse effect of

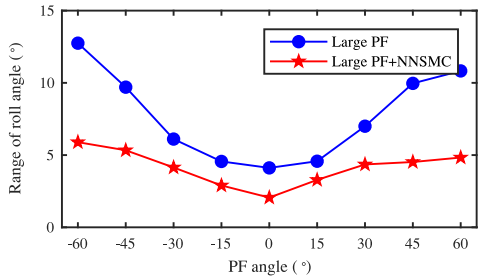

Fig. 8. Range of roll angle of the robotic fish with various PF angles during swimming with the TBF of 1.0 Hz.

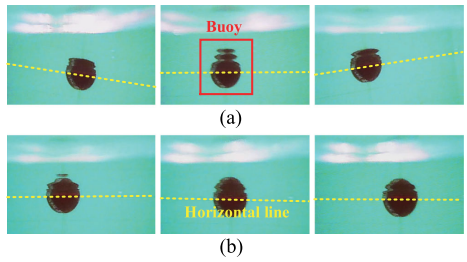

Fig. 9. Snapshot sequences in one cycle of fish tail, which are captured by the camera fixed on robotic fish. (a) Without reaction wheel. (b) With reaction wheel.

PF angle. It is revealed that the reaction wheel possesses better adaptability compared with PF.

D. Visual Stabilization Based on a Reaction Wheel

Since the initial motivation is to tackle the instability issue of onboard sensors, the video stability improved by the reaction wheel is demonstrated here. Fig. 9 displays the snapshot sequences in one cycle of fish tail, which are captured by the camera mounted on the fish head. The buoy in Fig. 9 is a red hallow sphere, which is a reference object. The yellow dashed lines represent the horizontal line. It is obvious that the image sequences in Fig. 9(b), corresponding to the system with reaction wheel, are much more stable than Fig. 9(a).

E. Discussion

The roll stability of robotic fish is critical to obtain the sensor data with low noise and perturbation, which will lay a solid foundation for environmental perception and autonomous operation. The proposal of the novel reaction-wheel-based stabilization method governs the roll stability of the robotic fish. In contrast to the passive stabilization based on PF, the proposed methods can achieve more significant effect for a wide scope of TBFs. Besides, the reaction wheel is mounted inside the robot, which does not rely on relative fluid motion to exert motion, so it adds little drag and unstable effect. Further, the neural network SMC is proposed to avoid the two kinds of disturbances from intrinsic motion and external fluid, the effectiveness of which is carefully demonstrated. Finally, visual experiments exhibit that a great improvement of image stability is obtained by the proposed methods, which may offer large convenience for the underwater visual perception and operation of the robotic fish.

Additionally, there are two phenomena worthy to be discussed. First, as shown in Figs. 5(c) and 7, the ranges of roll angle for 1.5 and 2.0 Hz TBFs are smaller than other cases. Besides, the systems without PF or with different-sized PFs exhibit the approximate stabilization performances for these two TBFs. One explanation could be that the time that fish body leans to one side is very short owing to the high frequency oscillation of fish tail, which means that the roll angle will be quickly corrected by self-motion. Therefore, the small roll angle is an inherent attribute for the case of high TBF, where the damping torque of PF only plays a minor role. Second, the stabilization performances of PF, PID, and SMC are not well received for 0.5 Hz TBF, which is depicted in Figs. 6(c) and 7. There are two possible reasons for these results. On the one hand, since the body angular velocity is low for 0.5 Hz TBF, the damping effect of PF is not significant. On the other hand, owing to the deformation of the posterior body, the mass distribution of robot changes inevitably, which leads to the corresponding change of the equilibrium point of roll angle. This adverse effect is more significant for slow deformation, which requires larger roll torque to avoid. Hence, the feedforward control is very essential to compensate this adverse effect.

Despite successfully implementing the roll stabilization with the reaction wheel, there is another issue to be addressed. The energy-saving control is a critical problem in the studies of robotic fish, but the energy consumption of the proposed methods is relatively large compared with the passive methods. Further studies will concentrate on the energy-optimal roll stabilization control.

VI. Conclusion

In this article, we have presented a roll stabilization control framework using a reaction wheel for the robotic fish. A novel robotic fish with an internal rotor and its dynamic model is built at first. By means of the dynamic model, the factors affecting roll stability are analyzed and the superiority of reaction-wheel-based stabilization method is demonstrated. Furthermore, the NNSMC is particularly designed to control the reaction wheel for better roll stability. Finally, the experimental results demonstrate that the stabilization performance of reaction wheel is obviously superior to that of the PF and the proposed NNSMC possesses impressive control effects. Remarkably, such results may lay a solid foundation for the environmental perception and autonomous operation of the underwater robots including robotic fish.

The ongoing and future work will focus on the energy-optimal roll stabilization control and implementing specific vision-based tasks by the robotic fish with reaction wheel, such as target tracking and pipeline inspection.

References

[1] M. Sfakiotakis, D. M. Lane, and J. B. C. Davies, "Review of fish swimming modes for aquatic locomotion," *IEEE J. Ocean. Eng.*, vol. 24, no. 2, pp. 237–252, Apr. 1999.

[2] F. E. Fish, "Advantages of natural propulsive systems," *Mar. Technol. Soc. J.*, vol. 47, no. 5, pp. 37–44, 2013.

[3] V. Kopman and M. Porfiri, "Design, modeling, and characterization of a miniature robotic fish for research and education in biomimetics and bioinspiration," *IEEE/ASME Trans. Mechatronics*, vol. 18, no. 2, pp. 471–483, Apr. 2013.

[4] Z. Wu, J. Liu, J. Yu, and H. Fang, "Development of a novel robotic dolphin and its application to water quality monitoring," *IEEE/ASME Trans. Mechatronics*, vol. 22, no. 5, pp. 2130–2140, Oct. 2017.

[5] W. Wang *et al.* "Three-dimensional modeling of a fin-actuated robotic fish with multimodal swimming," *IEEE/ASME Trans. Mechatronics*, vol. 23, no. 4, pp. 1641–1652, Aug. 2018.

[6] J. Yu, J. Liu, Z. Wu, and H. Fang, "Depth control of a bioinspired robotic dolphin based on sliding mode fuzzy control method," *IEEE Trans. Ind. Electron.*, vol. 65, no. 3, pp. 2429–2438, Mar. 2018.

[7] Y. Hu, W. Zhao, and L. Wang, "Vision-based target tracking and collision avoidance for two autonomous robotic fish," *IEEE Trans. Ind. Electron.*, vol. 56, no. 5, pp. 1401–1410, May 2009.

[8] Y. Takada, K. Koyama, and T. Usami, "Position estimation of small robotic fish based on camera information and gyro sensors," *Robotics*, vol. 3, no. 2, pp. 149–162, 2014.

[9] W. Wang and G. Xie, "Online high-precision probabilistic localization of robotic fish using visual and inertial cues," *IEEE Trans. Ind. Electron.*, vol. 62, no. 2, pp. 1113–1124, Feb. 2015.

[10] J. Yu, F. Sun, D. Xu, and M. Tan, "Embedded vision guided 3-D tracking control for robotic fish," *IEEE Trans. Ind. Electron.*, vol. 63, no. 1, pp. 355–363, Jan. 2016.

[11] F. Sun, J. Yu, P. Zhao, and D. Xu, "Tracking control for a biomimetic robotic fish guided by active vision," *Int. J. Robot. Autom.*, vol. 31, no. 2, pp. 137–145, 2016.

[12] X. Yang, Z. Wu, J. Liu, and J. Yu, "Design of a camera stabilizer system for robotic fish based on feedback-feedforward control," in *Proc. China Control Conf.*, Chengdu, China, Jul. 2016, pp. 6044–6049.

[13] M. Gajamohan, M. Muehlebach, T. Widmer, and R. D'Andrea, "The Cubli: A reaction wheel based 3D inverted pendulum," in *Proc. Eur. Control Conf.*, Zurich, Switzerland, Jul. 2013, pp. 268–274.

[14] M. Muehlebach and R. D'Andrea, "Nonlinear analysis and control of a reaction-wheel-based 3-D inverted pendulum," *IEEE Trans. Control Syst. Technol.*, vol. 25, no. 1, pp. 235–246, Jan. 2017.

[15] S. Han and J. Lee, "Balancing and velocity control of a unicycle robot based on the dynamic model," *IEEE Trans. Ind. Electron.*, vol. 62, no. 1, pp. 405–413, Jan. 2015.

[16] H. Jin, J. Hwang, and J. Lee, "A balancing control strategy for a one-wheel pendulum robot based on dynamic model decomposition: simulations and experiments," *IEEE/ASME Trans. Mechatronics*, vol. 16, no. 4, pp. 763–768, Aug. 2011.

[17] M. Zabihi and A. Alasty, "Dynamic stability and control of a novel handspringing robot," *Mech. Mach. Theory*, vol. 137, pp. 154–171, 2019.

[18] W. Whitacre, "An autonomous underwater vehicle as a spacecraft attitude control simulator," in *Proc. 43rd AIAA Aerosp. Sci. Meeting Exhibit*, 2005, doi: 10.2514/6.2005-137.

[19] J. Mayr, F. Spanlang, and H. Gattringer, "Mechatronic design of a self-balancing three-dimensional inertia wheel pendulum," *Mechatronics*, vol. 30, pp. 1–10, 2015.

[20] C. A. Woolsey and N. E. Leonard, "Stabilizing underwater vehicle motion using internal rotors," *Automatica*, vol. 38, no. 12, pp. 2053–2062, 2002.

[21] K. Morgansen, B. Triplett, and D. Klein, "Geometric methods for modeling and control of free-swimming fin-actuated underwater vehicles," *IEEE Trans. Robot.*, vol. 23, no. 6, pp. 1184–1199, Dec. 2007.

[22] J. Wang, Z. Wu, M. Tan, and J. Yu, "3-D path planning with multiple motions for a gliding robotic dolphin," *IEEE Trans. Syst., Man, Cybern., Syst.*, to be published, doi: 10.1109/TSMC.2019.2917635.

[23] J. Yu, Z. Wu, M. Wang, and M. Tan, "CPG network optimization for a biomimetic robotic fish via PSO," *IEEE Trans. Neural Netw. Learn. Syst.*, vol. 27, no. 9, pp. 1962–1968, Sep. 2016.

[24] Y. Shtessel, C. Edwards, L. Fridman, and A. Levant. *Sliding Mode Control and Observation*. New York. NY, USA, USA: Springer, 2014.

[25] A. Azar and Q. Zhu, *Advances and Applications in Sliding Mode Control Systems*. Berlin, Germany: Springer, 2015.

[26] S. Spurgeon, "Sliding mode control: A tutorial," in *Proc. Eur. Control Conf.*, Strasbourg, France, Jul. 2014, pp. 2272–2277.

[27] Y. Li, J. Zhang, and W. Qiong, *Adaptive Sliding Mode Neural Network Control for Nonlinear Systems*. San Francisco, CA, USA: Academic, 2019.

[28] J. Gao, X. An, A. Proctor, and C. Bradley, "Sliding mode adaptive neural network control for hybrid visual servoing of underwater vehicles," *Ocean Eng.*, vol. 142, no. 6, pp. 666–675, 2017.